Electronic structure of phospho-olivines Li_xFePO_4 ($x=0,1$) from soft-x-ray-absorption and -emission spectroscopies

A. Augustsson
Advanced Light Source, Lawrence Berkeley National Laboratory, Berkeley, California 94720 and Department of Physics, Uppsala University, Box 530, S-751201 Uppsala, Sweden

G. V. Zhuang
Materials Science Division, Lawrence Berkeley National Laboratory, Berkeley, California 94720

S. M. Butorin
Department of Physics, Uppsala University, Box 530, S-751201 Uppsala, Sweden

J. M. Osorio-Guillén
Department of Physics, Uppsala University, Box 530, S-751201 Uppsala, Sweden

C. L. Dong
Advanced Light Source, Lawrence Berkeley National Laboratory, Berkeley, California 94720 and Department of Physics, Tamkang University, Tamsui, Taiwan, Republic of China

R. Ahuja
Department of Physics, Uppsala University, Box 530, S-751201 Uppsala, Sweden

C. L. Chang
Department of Physics, Tamkang University, Tamsui, Taiwan, Republic of China

P. N. Ross
Materials Science Division, Lawrence Berkeley National Laboratory, Berkeley, California 94720

J. Nordgren
Department of Physics, Uppsala University, Box 530, S-751201 Uppsala, Sweden

J.-H. Guo[a)]
Advanced Light Source, Lawrence Berkeley National Laboratory, Berkeley, California 94720

(Received 18 July 2005; accepted 9 September 2005; published online 10 November 2005)

The electronic structure of the phospho-olivine Li_xFePO_4 was studied using soft-x-ray-absorption (XAS) and emission spectroscopies. Characteristic changes in the valence and conduction bands are observed upon delithation of $LiFePO_4$ into $FePO_4$. In $LiFePO_4$, the Fe-3*d* states are localized with little overlap with the O-2*p* states. Delithiation of $LiFePO_4$ gives stronger hybridization between Fe-3*d* states and O-2*p* states leading to delocalization of the O-2*p* states. The Fe *L*-edge absorption spectra yield "fingerprints" of the different valence states of Fe in $LiFePO_4$ and $FePO_4$. Resonant soft-x-ray-emission spectroscopy at the Fe *L* edge shows strong contributions from resonant inelastic soft x-ray scattering (RIXS), which is described using an ionic picture of the Fe-3*d* states. Together the Fe *L*-edge XAS and RIXS study reveals a bonding character of the Fe 3*d*-O2*p* orbitals in $FePO_4$ in contrast to a nonbonding character in $LiFePO_4$. © *2005 American Institute of Physics*.
[DOI: 10.1063/1.2107387]

I. INTRODUCTION

One of the most promising candidates to replace nickel or cobalt oxides as cathode materials in lithium-ion batteries is the phospho-olivine compound Li_xFePO_4. It has a high theoretical capacity (170 mA h/g). According to Refs. 1–3 this compound occurs in nature as the mineral *trihylite*, and is inexpensive, nontoxic, and nonhygroscopic. However, a possible drawback for practical application is its relatively low electronic conductivity ($\sim 10^{-9}$ S/cm). Various preparation procedures have been explored to overcome the low electronic conductivity, including coating or impregnating the particles with carbon[4] and supervalent doping,[5] although there is lingering controversy over the improved conductivity in the doped form of $LiFePO_4$. Therefore, detailed information on the electronic structure of $LiFePO_4$ and its electrochemically delithiated form, $FePO_4$, may be critical for future practical applications.

$LiFePO_4$ has orthorhombic crystal structure with *p-n-m-a* symmetry group and lattice constants of $a=10.329$ Å, $b=6.007$ Å, and $c=4.6908$ Å. Within the crystal structure, P atoms are coordinated with oxygen forming PO_4 tetrahedra, and Fe and Li atoms coordinated to oxygen atoms form FeO_6 and LiO_6 octahedra. The FeO_6 octahedra are in-

[a)]Electronic mail: jguo@lbl.gov

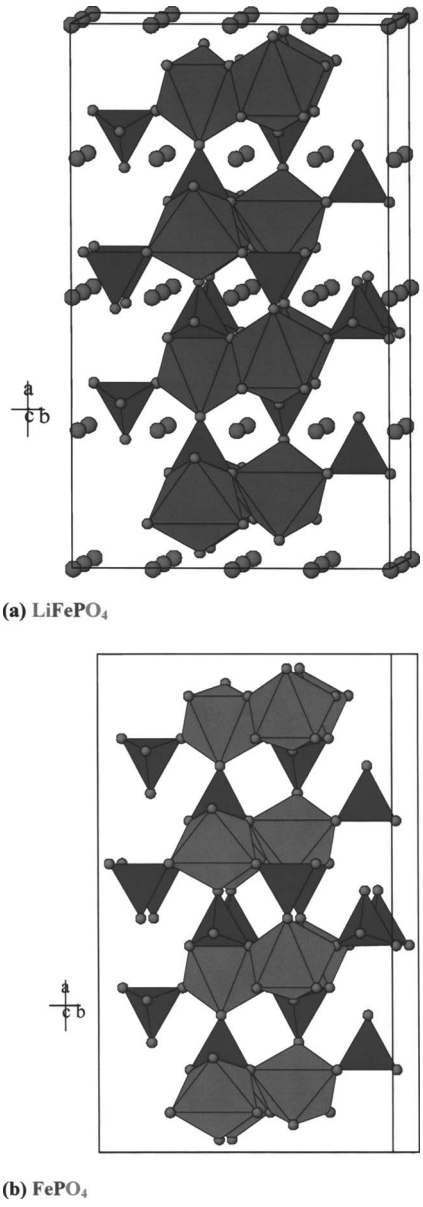

FIG. 1. Diagrams of the crystal structure of $LiFePO_4$ (a) and $FePO_4$ (b).

terconnected via corner sharing along the *bc* plane and have two common edges with the LiO_6 octahedra and one with the PO_4 tetrahedra. Chemical or electrochemical delithiation of olivine-$LiFePO_4$ results in $FePO_4$ or *heterosite*,[1,2] which maintains the original $LiFePO_4$ crystal structure with slightly smaller lattice constants (see Fig. 1). A previous x-ray diffraction (XRD) and Mössbauer spectroscopy[6] study of $LiFePO_4$ in electrochemical cell clearly showed that $LiFePO_4$ and $FePO_4$ coexist as two-phase $(1-x)LiFePO_4:(x)FePO_4$ at various states of lithium extractions (charge)/insertion (discharge). This two-phase nature of the system is believed to be an important fundamental property of this material in relation to its electrochemical performance as a Li-ion battery cathode. Therefore, to gain this fundamental understanding of the $LiFePO_4$ system, we studied the electronic structure of this system at fully charged state ($x \approx 0$) and fully discharged state ($x=1$), respectively.

The earlier studies of the electronic structure of the $LiFePO_4$ system have been within the framework of density-functional theory (DFT).[7] However, to our knowledge there is no experimental validation of the theoretical study. Recently, soft-x-ray-emission and -absorption spectroscopies have been applied successfully to study the electronic structure of various lithium intercalation systems, e.g., Li_xTiO_2,[8] vanadium nanotubes,[9] and $Li_xV_6O_{13}$.[10] The elemental and chemical sensitivities of the technique, due to involvement of both core and valence electrons, revealed strong electron correlation in the transition-metal (TM) 3*d* electrons and hybridization between oxygen and TM valence orbitals. Depending on the system, it can be described using a localized (ionic) picture of the 3*d* orbitals, a delocalized bandlike picture, or a combination of both localized and delocalized states.[11]

In this paper, the electronic structure of Li_xFePO_4 ($x=0$ and 1) was studied using soft-x-ray-absorption spectroscopy (XAS) and soft-x-ray-emission spectroscopy (XES). X-ray absorption and resonant x-ray emission at the Fe *L* edge and O *K* edge are presented. Resonant inelastic soft x-ray scattering (RIXS) at the Fe 2*p* edge is described using a localized picture. Crystal-field multiplet calculations were conducted to simulate the spectra. First-principles calculations, using density-functional theory, were made to describe the hybridization and simulated spectra and compared directly with experimental oxygen *K*-emission and absorption spectra.

II. EXPERIMENT

The experiments were performed at beamline 7.0.1 of Advanced Light Source, Lawrence Berkeley National Laboratory (LBNL). This beamline consists of a 5 m undulator and a spherical grating monochromator (SGM).[12] The measurements were performed at room temperature, with a base pressure in the experimental chamber lower than 5×10^{-9} mbar. XAS spectra were obtained by measuring the total electron yield (TEY) from the sample as a function of the incoming photon energy. All spectra were normalized to the photocurrent from a clean gold mesh introduced into the beam. A high-resolution grazing-incidence grating spectrometer[13] was used to record the emission spectra, with a resolution better than 0.75 and 0.4 eV for iron and oxygen, respectively. The resolution of the exciting photon beam was set to 0.2 and 0.3 eV for the O *K*-edge and Fe *L*-edge absorption measurements, respectively, and 0.4 and 0.75 eV for the O *K*-edge and Fe *L*-edge emission measurements. The spectrometer-detected photons were emitted parallel to the polarization vector of the incoming beam. The light incident angle was 40° with respect to the sample surface. Samples were introduced into the experimental chamber via a load lock. Loading of the samples into the load lock was done using a glove bag under argon flow to avoid contact with oxygen and moisture from the room atmosphere.

Battery grade (Hydro-Quebec) $LiFePO_4$ powder was used in this work. Olivine-type $FePO_4$ was prepared by chemically delithiation of the $LiFePO_4$ powder by using the following procedures: (a) 3.14 g of $LiFePO_4$ powder was suspended in 10 ml of dry acetonitrile (CH_3CN), (b) a bromine solution was separately prepared by dissolving bromine

in 10 ml dry CH_3CN, (c) the bromine solution was added into the $LiFePO_4$ suspension dropwise, and (d) the mixture was stirred overnight. The lithium bromide and traces of unreacted bromine were removed from the $FePO_4$ by filtration. After the first treatment, x-ray powder diffraction (XRPD) analysis showed that the sample is primarily *o*-$FePO_4$, with 11% $LiFePO_4$ remaining. The treatment was repeated till the $LiFePO_4$ remaining was reduced to 2% as determined by XRD.

III. CALCULATION METHODS

Two different theoretical models were used, crystal-field multiplet theory and DFT. Crystal-field multiplet theory has been successfully applied to TM compounds with strong electron correlation and can reproduce both XAS and resonant XES/RIXS at the 3*d* metal site.[14,15] But the ionic multiplet approach only partly included the effects of chemical bonding, and could not be used to describe the oxygen XAS and XES spectra. On the other hand density-functional theory describes the hybridization between the elements well, but at present there are no well-developed formulations to simulate resonant x-ray emission. Therefore, O 2*p* occupied and unoccupied densities of states (DOS) obtained from DFT were used and compared with oxygen absorption and normal x-ray-emission spectra, respectively.

A. Density-functional theory calculation

First-principles investigation using DFT within the full-potential linear-muffin-tin-orbital (FP-LMTO) method[16] was used to calculate the lithiated ($x=1$) and delithiated ($x=0$) phases of Li_xFePO_4.[17] We made use of the pseudocore 3*p* states for Fe, and valence band 2*s*, 2*p*, and 3*s* basis functions for Li, valence band 3*d*, 4*s*, 4*p*, and 4*d* basis functions for Fe, valence band 3*s*, 3*p*, 4*s*, and 3*d* basis functions for P, and valence band 2*s*, 2*p*, and 3*s* basis functions for O with two corresponding sets of energy parameters, one appropriate for the semicore 3*d* states, and the other appropriate for the valence states. The resulting basis formed a single, fully hybridized basis set. This approach has been previously proven to give a well-converged basis.[16] For the sampling of the irreducible wedge of the Brillouin zone, we used the special ***k***-point method.[18] In order to speed up the convergence, we applied a Gaussian broadening of a width of 20 mRy to each calculated eigenvalue.

B. Crystal-field multiplet calculations

The single-particle description of x-ray absorption works well for *K* edges of all transition-metal oxides and a range of dedicated computer codes exist to calculate the x-ray-absorption spectra.[19,20] However, for the other edges, in particular, the metal $L_{2,3}$ edges, the agreement is poor. The reason for the discrepancy is not that the density of states is calculated incorrectly, but that one does not observe the density of states directly in the x-ray-absorption processes.[21] Multiplet effects play an important role when a core hole in the *L* shell is present. Ligand field multiplet theory[22] calculations were performed using Cowan's[23] and Butler's[24] codes, which were modified by Thole *et al.*[25] In this approach, the interelectronic repulsions are introduced through Slater integrals, describing 3*d*-3*d* and 3*d*-2*p* Coulomb and (super) exchange interactions. Slater integrals and spin-orbit constants were obtained by the Hartree-Fock method.[23] The effect of electron delocalization and covalency of the chemical bonds was taken into account by scaling the Slater integrals to 80%. The octahedral coordination around the Fe atom is represented by the crystal-field parameter $10D_q$, although the calculations were done in the basis of C_s symmetry. The lifetime ω_i of the intermediate state was set to 0.2 and 0.3 eV for Fe L_3 and Fe L_2, respectively. The Fe *L*-edge RIXS spectra were calculated as a coherent second-order optical process, including interference effects, using the Kramer-Heisenberg formula[26]

$$I(\Omega,\omega)=\sum_f \left| \sum_i \frac{\langle f|\hat{D}_q|i\rangle\langle i|\hat{D}_q|g\rangle}{E_g+\Omega-E_i-i\Gamma_i/2} \right|^2 \delta(E_g+\Omega-E_f-\omega),$$

where Ω and ω represent the energies of the incident and scattered photons; and $|g\rangle$, $|i\rangle$, and $|f\rangle$ are ground, intermediate and final states with energies E_g, E_i, and E_f; and D_q is the dipole operator. The lifetime broadening of each intermediate state, which gives rise to an interference effect, was represented by Lorenzian model with full width half maximum Γ_i.

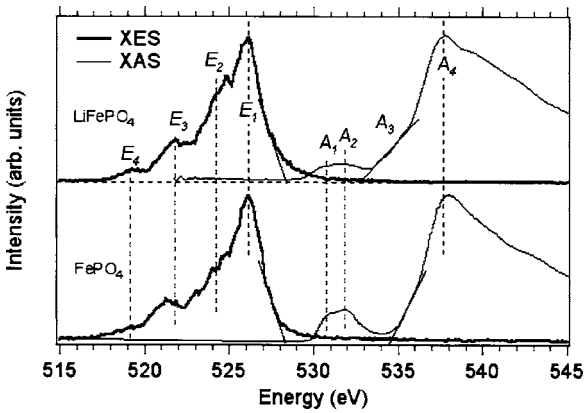

FIG. 2. X-ray absorption-emission spectra of $FePO_4$ and $LiFePO_4$.

IV. RESULTS AND DISCUSSION

A. The O *K* edge

The O *K*-edge absorption and emission spectra of $FePO_4$ and $LiFePO_4$ are plotted on a common energy scale in Fig. 2. The oxygen XES and XAS spectra, to a first-order approximation, reflect the occupied and unoccupied oxygen-*p* projected densities of states, respectively. Both XES spectra of $FePO_4$ and $LiFePO_4$ show four resolved emission bands with some differences in the intensity distribution and central weight for bands E_1 and E_3. An increase in intensity of E_2 is observed in $LiFePO_4$, while the deeper emission band E_4 is less affected by Li intercalation. A small weight of enhancement is also found at the top of the valence band (starting from 528 eV) of $LiFePO_4$. X-ray-absorption spectra show a main threshold starting from absorption feature A_4 for both $FePO_4$ and $LiFePO_4$. The preedge absorption features are indicated as A_1 and A_2, which are clearly resolved in $FePO_4$ in contrast to a broadband in $LiFePO_4$. The nature of the

absorption features of A_1 and A_2 will be interpreted in the later paragraph. A notable intensity increase in the region of A_3 is also observed in $LiFePO_4$, which is probably related to the Li intercalation, similar to the Li-doped $Li_xNi_{1-x}O$ systems.[27]

The previous studies show in some cases that a combined x-ray absorption-emission spectrum offers an alternative method for measuring the band gaps of insulators and semiconductors.[28–30] However, it seems to be more difficult to determine the band gap in $FePO_4$ and $LiFePO_4$ from current XAS and XES study. The determination of the top of the valence band is clear as indicated in Fig. 2. If one assigns the Fe-3*d*–O-2*p* hybridized states to be the bottom of the conduction band, the band gap obtained would be 1.7 and 0.5 eV for $FePO_4$ and $LiFePO_4$, respectively. But if one assigns the Li-derived state in O *K*-edge absorption spectrum of $LiFePO_4$ to be the bottom of the conduction band, a band gap of 4.0 eV is obtained for $LiFePO_4$, which agrees well with the theoretical value based on GGA+U by Zhou *et al.*[31] Thus, the states in the band gap of $LiFePO_4$ (indicated as A_1 and A_2 in x-ray-absorption spectrum) would be excitonic in nature.

As the outer valence bands of both $LiFePO_4$ and $FePO_4$ are formed from O-2*p* and Fe-3*d* states, the nature of hybridization in the valence band could be measured and compared with the DFT calculation. Figure 3 shows the calculated total DOS of $LiFePO_4$ and $FePO_4$ for the occupied and unoccupied contributions along with the partial density of states of Fe-*d* state, O-*p* state, P-*p* state, and Li-*s* and *p* states. Since major contributions to the total DOS come from Fe-*d* states and O-*p* states, it is informative to more closely examine such states in $LiFePO_4$ and $FePO_4$. The difference between the two systems, Li_xFePO_4 ($x=0,1$), lies in the extent of hybridization and intensity distribution across the whole valence band. For the occupied DOS of $FePO_4$, there is a strong overlap between Fe-3*d* and O-2*p* states and the overlapping states are distributed across the whole valence band in $FePO_4$, while the valence band within 3 eV of top in $LiFePO_4$ is predominately Fe-3*d* with a small contribution of O-2*p*–Fe-3*d* states. On the other hand, the bottom of the conduction band (within 2 eV of the edge) is dominated by Fe-3*d* states in both $LiFePO_4$ and $FePO_4$, with the exception that the unoccupied Fe-3*d* states in $FePO_4$ present more mixing with O-2*p* states in the bottom of conduction band than that of $LiFePO_4$.

Oxygen *K*-edge absorption (upper panel) and emission spectra (lower panel) of $FePO_4$ and $LiFePO_4$ are displayed along with the calculated unoccupied and occupied DOS in Figs. 4 and 5, respectively. All experimental spectra are normalized to peak maximum, and theoretical unoccupied DOS are shifted in energy to coincide with the corresponding experimental data. The oxygen 2*p* partial-DOS curves of $LiFePO_4$ and $FePO_4$ are shifted to 530.5 and 527.5 eV, respectively. Although the FP-LMTO approach has limitations due to its approximate nature in treating electron correlation as discussed by Zhou *et al.*,[31] the calculated occupied and unoccupied DOS (in Fig. 3) yield reasonable agreement with experiment.

As shown in Figs. 4 and 5, the oxygen XAS spectra of

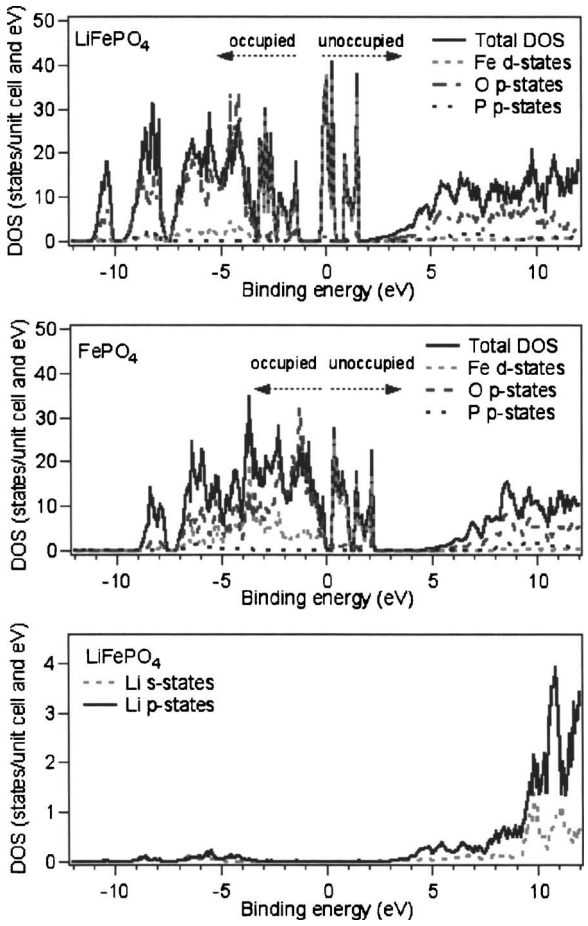

FIG. 3. Total and partial density of states for oxygen *p*, iron *d*, phosphor *p*, and lithium *s* and *p* of $LiFePO_4$ and $FePO_4$ obtained from DFT calculations.

both $LiFePO_4$ and $FePO_4$ can be divided into two regions. First, the well-defined preedge is attributed to O 2*p* weighting of states that have predominantly transition-metal 3*d* character,[32] i.e., Fe-3*d*–O-2*p* mixing. Interestingly, the mixing is found to be more substantial in $FePO_4$ than in $LiFePO_4$. The 3*d* states are split into two bands, which are related to t_{2g} and e_g symmetries, although this assignment is not strictly valid as the crystal field is slightly distorted from octahedral symmetry. The second region, about 5–10 eV above the threshold, is attributed to O-2*p* character hybridized with Fe-4*s* and 4*p* states. A similar trend has been observed in oxygen *K*-edge XAS of pure Fe-oxide compounds,[32] such as $Fe_2O_3(Fe^{3+})$ and $FeO(Fe^{2+})$, except that the Fe oxides give rise to substantially more weight in the preedge region in comparison to the Fe-phosphates. The relative intensity ratio of the preedge region to that of the second region is attributed to number of unoccupied Fe-3*d* states and the degree of hybridization between Fe-3*d* and O-2*p* states. O *K*-edge absorption spectra clearly revealed that hybridization between Fe-3*d* and O-2*p* states in phospho-olivines $LiFePO_4$ and $FePO_4$ is much less extensive than that in iron oxides. In addition, such hybridization is found to be weaker in $LiFePO_4$ than in $FePO_4$. The DFT calculations show that the energy separation between occupied and unoccupied O-*p* DOS becomes smaller upon

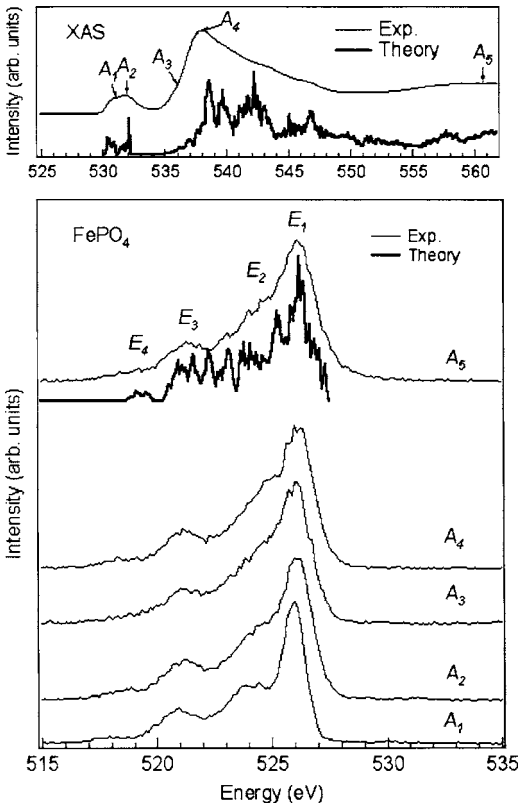

FIG. 4. Top panel: the O *L*-edge absorption spectrum of $LiFePO_4$ and DFT calculated unoccupied DOS. Bottom panel: resonant oxygen *K* emission of $LiFePO_4$ and DFT calculated occupied DOS, and resonant O *K*-emission spectra recorded at selected excitation energies.

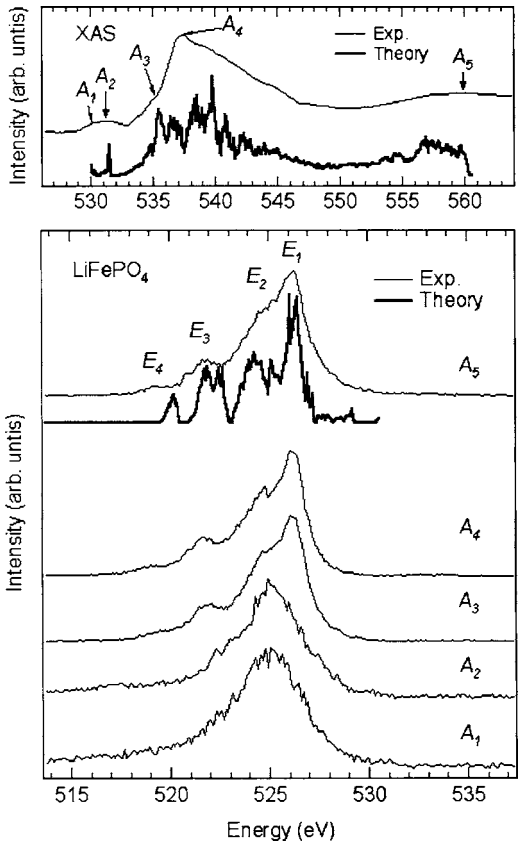

FIG. 5. Top panel: the O *L*-edge absorption spectrum of $FePO_4$ and DFT calculated unoccupied DOS. Bottom panel: resonant oxygen *K* emission of $LiFePO_4$ and DFT calculated occupied DOS, and resonant O *K*-emission spectra recorded at selected excitation energies.

delithiation as a result of band gap narrowing, consistent with increasing the over all hybridization between O-2*p* and Fe-3*d* states in $FePO_4$.

O *K*-emission spectra of $FePO_4$ and $LiFePO_4$ (thin lines) are shown in lower panel in Figs. 4 and 5, respectively. The normal emission spectra (excited at point A_5) are compared with occupied O-*p* partial DOS calculations (thick line). The oxygen emission spectra consist of four bands: a high-energy "main" band centered around 526 eV (E_1), a strong shoulder (E_2) on its low-energy side, followed by a weaker lobe (E_3), and a tail (E_4). Calculated O-occupied *p* partial DOS are in excellent agreement with emission spectra of $FePO_4$ and $LiFePO_4$ (curve A_5 in lower panel of Figs. 4 and 5). The assignment of each band can be easily made with reference to the occupied oxygen partial DOS and its overlap with partial DOS of Fe, P across the whole valence band (see Fig. 3). The main band (E_1) and its shoulder (E_2) are originated from O-2*p* and Fe-3*d* derived states. Emission from the deeper inner bands E_3 and E_4 is given rise by some O-2*p* hybridization with Fe-3*d* and also with P-*p*, Li-*s*, and Li-*p*, respectively.

The resonant x-ray-emission spectra of $FePO_4$ and $LiFePO_4$ are also presented in Figs. 4 and 5. In Fig. 4, the four resonantly excited O *K*-emission spectra (curves A_1-A_4) show that the four-band spectral profiles are very similar to the normal emission spectrum (A_5). The narrowing of the XES feature E_1 in spectra A_1 and A_2 could be attributed to the fact that only O-2*p* bands admixed to Fe-3*d* are selected at these excitation energies. The similarity of the resonantly excited XES spectra of $FePO_4$ indicates that the oxygen atoms are all in equivalent sites.[28,33] In contrast, for $LiFePO_4$ (in Fig. 5), the resonant XES spectra A_1 and A_2 are very different from A_3 and A_4. One possible interpretation could be that oxygen atoms are at inequivalent sites due to the intercalation of Li ions in the crystal structure of $LiFePO_4$. The clear difference between the preedge excited spectra of $LiFePO_4$ and $FePO_4$ points changes in hybridization. The DFT calculation suggests that Li-*s* and *p* states are situated in this energy range, which could give rise to the changes in hybridization observed in $LiFePO_4$ upon delithiation.

The direct comparison of O *K*-edge emission spectra between $FePO_4$ and $LiFePO_4$ is displayed in Fig. 6 (curves A_1 and A_5). The normal emission spectra (A_5) reveal the increasing in O-2*p* and Fe-3*d* hybridization upon delithiation, as evidenced by the intensity decrease of the emission band E_2 and the shift of the emission band E_3 in $FePO_4$. Also observed in Fig. 6 is the striking resonant x-ray-emission spectral difference as the excitation energy is tuned to the preedge in the absorption spectrum (A_1), i.e., resonant excitation to Fe-3*d*–O-2*p* derived states. In $LiFePO_4$ the emission band at 525 eV becomes the dominant feature, whereas in the delithiated phase ($FePO_4$) the resonant O *K*-emission spectrum resembles the spectral profile of the normal emission spectrum that reflects the partial density of states.

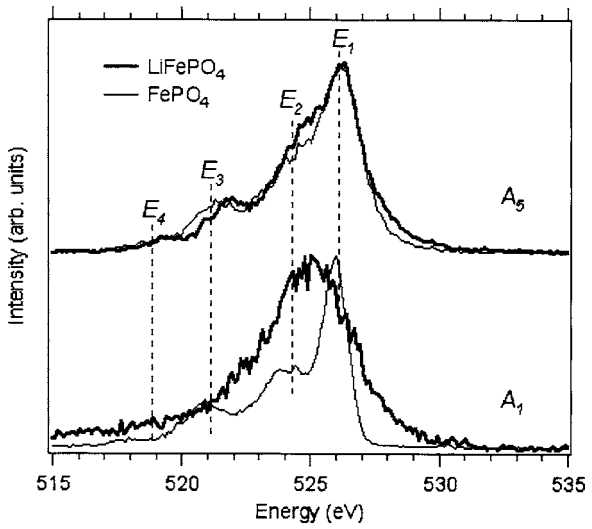

FIG. 6. The resonant and normal O *K*-emission spectra of $FePO_4$ and $LiFePO_4$.

B. The Fe 2*p* edge

X-ray-absorption spectra of $LiFePO_4$ and $FePO_4$ are presented in upper panels of Figs. 7 and 8. Fe $L_{2,3}$-absorption features in $LiFePO_4$ are allocated in between 706 and 725 eV, with a spin-orbit splitting of ~13 eV. Similar splitting is also found in XAS spectrum of $FePO_4$, presented in the upper panel of Fig. 8. The splitting and intensity ratios observed for either Fe L_2 or Fe L_3 edge in absorption spectra arise from the interplay of crystal-field and electronic interactions, and are not directly related to the splitting of Fe-3*d* orbitals into t_{2g} and e_g subsets.[34] The observed main peak shifts to 710 eV in $FePO_4$ relative to 708 eV in $LiFePO_4$ and overall spectral changes compared to $LiFePO_4$ are due to the valence change from Fe^{3+} to Fe^{2+} and the increase in crystal-field strength.

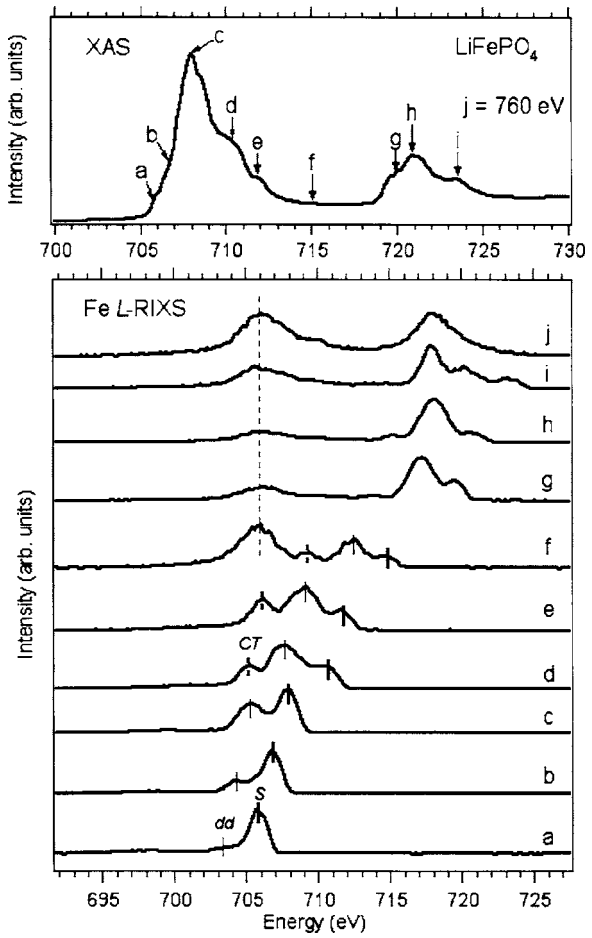

FIG. 7. Top panel: the Fe *L*-edge XAS spectra of $LiFePO_4$. Bottom panel: resonant Fe *L*-emission spectra recorded at selected excitation energies.

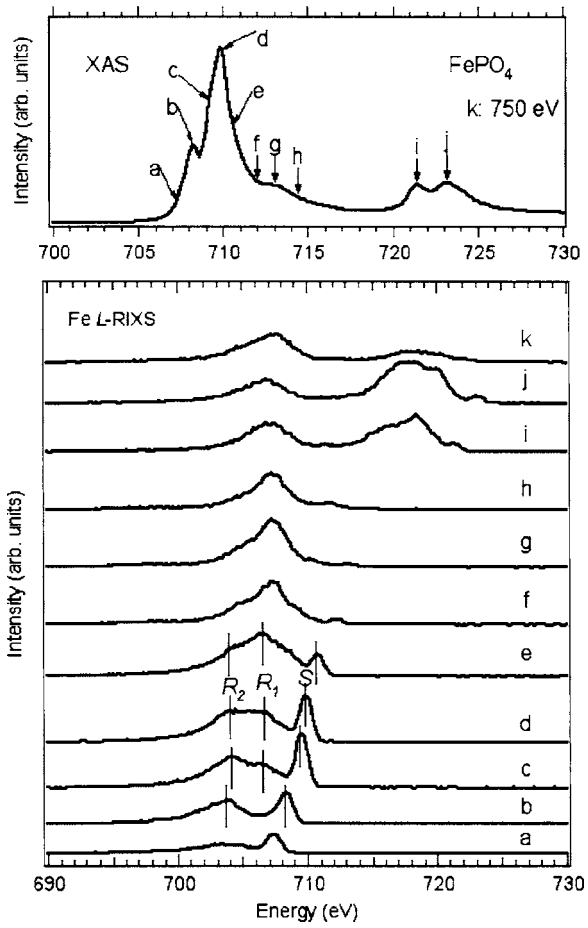

FIG. 8. Top panel: the Fe *L*-edge XAS spectra of $FePO_4$. Bottom panel: resonant Fe *L*-emission spectra recorded at selected excitation energies.

When the excitation energy is tuned to the different features in the absorption spectra, the RIXS spectra of $LiFePO_4$ and $FePO_4$ are found to exhibit resonant energy-loss structures due to both *d-d* excitations of Raman scattering and charge-transfer excitations of final-state character. Resonant x-ray-emission spectra of $LiFePO_4$ and $FePO_4$, shown in Figs. 7 and 8, were recorded at selected excitation energies (denoted by letters *a*–*i*) near the Fe L_3 and L_2-absorption resonances. Normal emission spectra (curve *j* in Figs. 7 and 8) are from Fe *L* emission obtained at excitation energy of 760 eV. The resonant XES spectra are displayed on emission photon energy scale and normalized to the peak maximum to emphasize changes in the spectral profile upon the increasing excitation energy. Clearly, emission intensity distributions show strong dependence on the incoming excitation photon energy. All the spectra consist of three different contributions:[14] recombination (also called elastic) peak,

resonant energy-loss (also called inelastic) features mostly due to *d-d* excitations as well as due to the charge-transfer excitations, and normal x-ray emission. The elastic and inelastic contributions disperse with photon energy as a consequence of energy conservation while the normal emission is nondispersive.

For the resonant Fe *L*-emission spectra of $LiFePO_4$ in Fig. 7, the *d-d* excitation feature (*dd*) shifts towards higher photon energy commensurate with the increasing energy of the elastic peak (*S*). Another energy-loss feature (charge-transfer excitation) appears when the excitation energy is set to the 710.5 eV absorption resonance (curve *d*). The normal emission contribution is found at the constant photon energy (indicated by vertical dash line) when the excitation energy is above the ionization threshold of Fe L_3 edge (starting from curve *f*). In contrast, the resonant Fe *L*-emission spectra of $FePO_4$ (see in Fig. 8) exhibit quite different behavior. For the excitation energies near the L_3- and L_2-absorption resonances (curves $a-j$ in Fig. 8), the Fe *L*-emission spectral distribution is much broader in comparison with that of $LiFePO_4$. The normal emission contribution is discernable already in spectra at photon excitation energy as low as 712 eV (curve *f* in Fig. 8). The large contribution of normal emission in the spectra of $LiFePO_4$ is interpreted as delocalization of Fe-3*d* states, a consequence of significantly increased hybridization between the Fe-3*d* states and O-2*p* states. At lower excitation energies (curves $a-e$), the x-ray emission does not exhibit dispersive behavior as the excitation energy increases. The possibility of nonlinear dispersion in inelastic scattering features, corresponding to charge-transfer excitations, has been discussed in the RIXS spectra of CoO.[14] It was shown that as the excitation energy tuned to the region of charge-transfer satellites in the absorption spectrum (in this case, intermediate states of mainly $2p^5 3d^{n+2}L$ character), no correlation between the incident and emitted photon energies could be observed, so that the charge-transfer structure behaves as a normal-emission-like line.

The calculated XAS spectra of $LiFePO_4$ and $FePO_4$ are compared with the experimental ones in upper panels of Figs. 9 and 10. The multiplet ligand theory calculations reproduce the observed spectra using crystal-field strengths of 0.5 and 1.45 eV for $LiFePO_4$ and $FePO_4$, respectively. The crystal-field strengthening found in $FePO_4$ is also consistent with a slight Fe–O bond distance decrease upon delithiation.[6] It is known that the multiplet interaction is very strong in TM *L*-edge XAS. For example, in 3*d* transition-metal compounds, the 3*d*-3*d* and the 2*p*-3*d* interactions are most important for the description of the *L*-edge absorption spectrum.[35] It is these two-particle interactions that define the ground state of the transition-metal ion, and that split the XAS final state into a large number of configurations (multiplets). Furthermore, the Fe-2*p* core hole-3*d*-electron multiplet interactions are responsible for the whole shape of the XAS in Fe_2O_3 and FeO.[36] The agreement between the XAS spectra and multiplet calculations in Figs. 9 and 10 reflects the ionic nature of the Fe^{2+} and Fe^{3+} in $LiFePO_4$ and $FePO_4$.

Resonant Fe *L*-emission spectra (resonant inelastic x-ray scattering spectra) of $LiFePO_4$ and $FePO_4$ are plotted on the energy-loss scale and compared with the crystal-field multiplet calculations as well in Figs. 9 and 10, in which the energy-loss scale was obtained by subtracting the excitation energy from each spectrum. To facilitate comparison of theory and experiment, the corresponding theoretical RIXS spectra of Fe^{2+} and Fe^{3+} were shifted by −2 and −3.7 eV, respectively, to align with the experimental spectra. The experimental RIXS spectra recorded at selected excitations (curves $a-i$ in Figs. 9 and 10) were well reproduced by the multiplet ligand theory calculations, although the normal emission contribution was not included in crystal-field multiplet calculations. In Fig. 9, the calculation indicates that prominent inelastic features at −2.5 and −5.5 eV below the recombination peak correspond to *d-d* excitations in $LiFePO_4$. The distinctive RIXS features reveal that Fe 3*d* electrons in $LiFePO_4$ are highly localized. For $FePO_4$ in Fig. 10, a broad structure is found around the range of −2 to −8 eV, e.g., see spectra $a-f$. This structure could be attributed to charge-transfer excitations, i.e., ligand 2*p* to metal 3*d* transfer.[37] The broad RIXS features in $FePO_4$ have O-2*p* band character indicating a stronger bonding interaction between Fe-3*d* and O-2*p* states in the delithiated material.

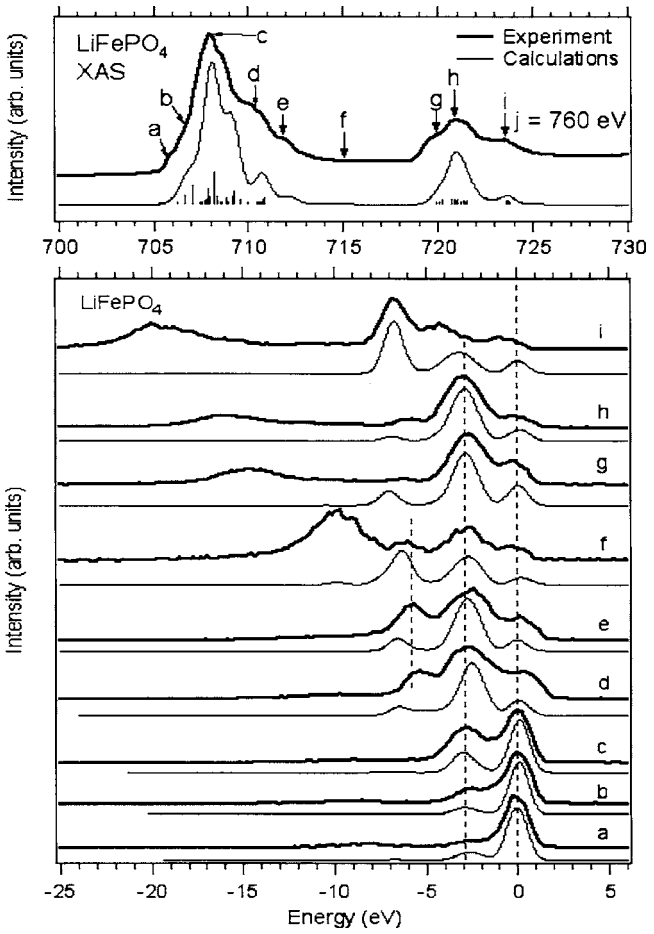

FIG. 9. Top panel: the experimental and theoretical Fe *L*-edge XAS spectra of $LiFePO_4$. Bottom panel: the experimental and theoretical Fe *L*-edge RIXS spectra of $LiFePO_4$, and the theoretical RIXS spectra of $LiFePO_4$ are shifted by −2 eV.

V. SUMMARY

Soft x-ray spectroscopy was used to investigate the electronic structure of $LiFePO_4$ and $FePO_4$. Experimental spectra

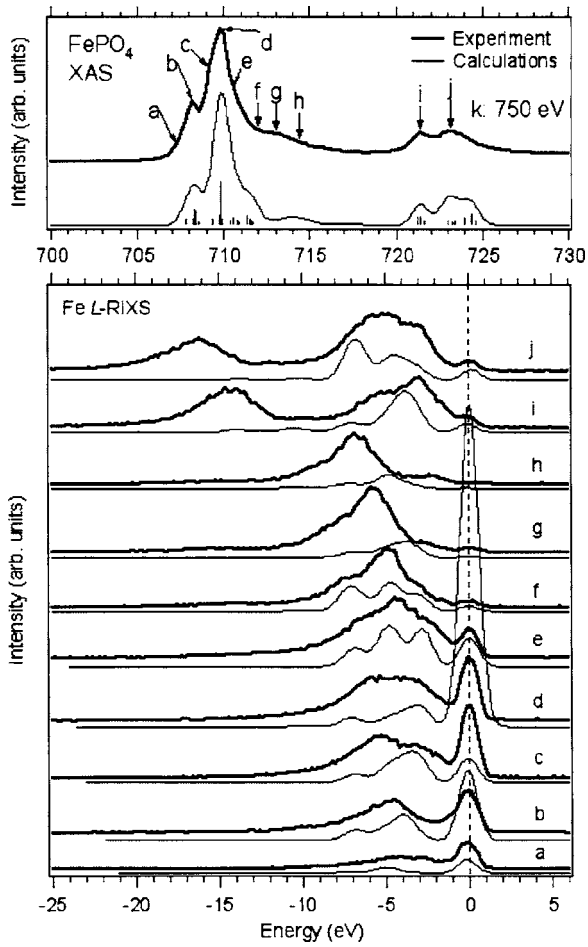

FIG. 10. Top panel: the experimental and theoretical Fe *L*-edge XAS spectra of $FePO_4$. Bottom panel: the experimental and theoretical Fe *L*-edge RIXS spectra of $FePO_4$, and the theoretical RIXS spectra of $LiFePO_4$ are shifted by −3.7 eV.

were compared with the theoretical calculations: the partial density of states calculations using density-functional theory and local excitations within Fe-3*d* states simulated using crystal-field multiplet theory. In $LiFePO_4$, localized Fe-3*d* states are only slightly hybridized with O-2*p* states at the top of valence band. When lithium is extracted, the O-2*p* states shift into the band gap leading to stronger bonding between Fe-3*d* states and O-2*p* states and to delocalization of the O-2*p* states. Resonant soft-x-ray emission spectroscopy at the Fe *L* edge shows strong contributions from inelastic scattering (RIXS), which is described using an ionic picture of the Fe-3*d* states. Together the Fe *L*-edge XAS and RIXS study reveals a bonding character of the Fe-3*d*–O-2*p* orbitals in $FePO_4$ in contrast to a nonbonding character in $LiFePO_4$. The electron transport in both materials is expected to be polaronic in nature.

ACKNOWLEDGMENTS

This work was supported by the Swedish Natural Science Research Council (VR), and by the Göran Gustafsson Foundation for Research in Natural Science and Medicine (GGS). The work at the Advanced Light Source (ALS) and Chemical Science Division (GVZ and PNR) is supported by the Office of Basic Energy Science, Material Science Division, of the US Department of Energy under Contract No. DE-AC02-05CH11231. Discussions with Professor G. Ceder (MIT) on phospho-olivines band gap are greatly appreciated. We thank Dr. Tom Richardson for supplying the chemically delithiated $FePO_4$.

[1] A. K. Padhi, K. S. Nanjundaswamy, C. Masquelier, S. Okada, and J. B. Goodenough, J. Electrochem. Soc. **144**, 1609 (1997).
[2] A. K. Padhi, K. S. Nanjundaswamy, and J. B. Goodenough, J. Electrochem. Soc. **144**, 1188 (1997).
[3] A. Yamada, S. C. Chung, and K. Hinokuma, J. Electrochem. Soc. **148**, A224 (2001).
[4] H. Huang, S.-C. Yin, and L. F. Nazar, Electrochem. Solid-State Lett. **4**, A170 (2001); P. P. Prosini, D. Zane, and M. Pasquali, Electrochim. Acta **46**, 3517 (2001).
[5] S.-Y. Chung, J. T. Blocking, and Y.-M. Chiang, Nat. Mater. **1**, 123 (2002).
[6] A. S. Andersson, B. Kalska, L. Häggström, and J. O. Thomas, Solid State Ionics **130**, 41 (2000).
[7] A. Yamada and S.-C. Chung, J. Electrochem. Soc. **148**, A960 (2001); P. Tang and N. A. W. Holzwarth, Phys. Rev. B **68**, 165107 (2003).
[8] A. Augustsson, A. Henningsson, S. M. Butorin, H. Siegbahn, J. Nordgren, and J.-H. Guo, J. Chem. Phys. **119**, 3983 (2003).
[9] A. Augustsson, T. Schmitt, L.-C. Duda, J. Nordgren, S. Nordlinder, K. Edstrom, T. Gustafsson, and J.-H. Guo, J. Appl. Phys. **94**, 5083 (2003).
[10] T. Schmitt, A. Augustsson, L.-C. Duda, J. Nordgren, J. Höwing, and T. Gustafsson, J. Appl. Phys. **95**, 6444 (2004).
[11] T. Schmitt, L.-C. Duda, M. Matsubara *et al.*, Phys. Rev. B **69**, 125103 (2004).
[12] T. Warwick, P. Heimann, D. Mossessian, W. McKinney, and H. Padmore, Rev. Sci. Instrum. **66**, 2037 (1995).
[13] J. Nordgren, G. Bray, S. Cramm, R. Nyholm, J.-E. Rubensson, and N. Wassdahl, Rev. Sci. Instrum. **60**, 1690 (1989).
[14] S. Butorin, J. Electron Spectrosc. Relat. Phenom. **110-111**, 213 (2000).
[15] A. Kotani and S. Shin, Rev. Mod. Phys. **72**, 621 (2000).
[16] M. Wills, O. Eriksson, and M. Alouani, in *Electronic Structure and Physical Properties of Solids: The Uses of the LMTO Method*, edited by Hugues Dreysse (Springer, Berlin, 2000).
[17] J. M. Osorio-Guillén, B. Holm, R. Ahuja, and B. Johansson, Solid State Ionics **167**, 221 (2004).
[18] D. J. Chadi and M. L. Cohen, Phys. Rev. B **8**, 5747 (1973); S. Froyen, *ibid.* **39**, 3168 (1989).
[19] J. J. Rehr and R. C. Albers, Rev. Mod. Phys. **72**, 621 (2000).
[20] J. J. Rehr and A. L. Ankudinov, J. Synchrotron Radiat. **8**, 61 (2001).
[21] F. M. F. de Groot, Coord. Chem. Rev. **249**, 31 (2005).
[22] See, e.g., *Ligand-Field Theory and its Applications*, edited by B. N. Figgs and M. A. Hitchman (Wiley-VCH, New York, 2000); *Introduction to Ligand Field Theory*, edited by C. J. Ballhausen (McGraw-Hill, New York, 1962).
[23] *The Theory of Atomic and Structure and Spectra*, edited by R. D. Cowan (University of California Press, Berkeley, CA, 1981).
[24] *Point Group Symmetry Applications: Methods and Tables*, edited by P. H. Butler (Plenum, New York, 1981).
[25] B. T. Thole, G. van der Laan, and P. H. Butler, Chem. Phys. Lett. **149**, 295 (1988).
[26] H. A. Kramers and W. Heisenberg, Z. Phys. **31**, 681 (1925).
[27] P. Kuiper, G. Kruizinga, J. Ghijsen, G. A. Sawatzky, and H. Verweij, Phys. Rev. Lett. **62**, 221 (1989).
[28] J.-H. Guo, S. M. Butorin, N. Wassdahl, J. Nordgren, P. Berastegut, and L.-G. Johansson, Phys. Rev. B **61**, 9140 (2000).
[29] C. L. Dong, C. Persson, L. Vayssieres, A. Augustsson, T. Schmitt, M. Mattesini, R. Ahuja, C. L. Chang, and J.-H. Guo, Phys. Rev. B **70**, 195325 (2004).
[30] J. Luning, J. Rockenberger, S. Eisebitt, J.-E. Rubensson, A. Karl, A. Kornowski, H. Weller, and W. Eberhardt, Solid State Commun. **112**, 5 (1999).
[31] F. Zhou, K. Kang, T. Maxisch, G. Ceder, and D. Morgan, Phys. Rev. B **70**, 235121 (2004); F. Zhou, K. Kang, T. Maxisch, G. Ceder, and D. Morgan, Solid State Commun. **132**, 181 (2004).

[32] F. M. F. de Groot, M. Grioni, J. C. Fuggle, J. Ghijsen, G. A. Sawatzky, and H. Petersen, Phys. Rev. B **40**, 5715 (1989).
[33] J.-H. Guo, S. M. Butorin, N. Wassdahl, P. Skytt, J. Nordgren, and Y. Ma, Phys. Rev. B **49**, 1376 (1994).
[34] G. van der Laan and I. W. Kirkman, J. Phys.: Condens. Matter **4**, 4189 (1992).
[35] F. M. F. De Groot, J. C. Fuggle, B. T. Thole, and G. A. Sawatzky, Phys. Rev. B **42**, 5459 (1990).
[36] J. P. Crocombette, M. Pollak, F. Jollet, N. Thomat, and M. Gautier-Soyer, Phys. Rev. B **52**, 3143 (1995).
[37] S. M. Butorin, J.-H. Guo, M. Magnuson, and J. Nordgren, Phys. Rev. B **55**, 4242 (1997).